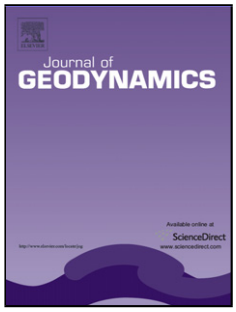

Title: Geodynamic origin of carbonatites from the absolute paleotectonic reconstructions

Authors: Liya N. Kogarko, Roman V. Veselovskiy

PII: S0264-3707(18)30170-4
DOI: https://doi.org/10.1016/j.jog.2019.01.017
Reference: GEOD 1625

To appear in: *Journal of Geodynamics*

Received date: 16 June 2018
Revised date: 10 January 2019
Accepted date: 27 January 2019

Please cite this article as: Kogarko LN, Veselovskiy RV, Geodynamic origin of carbonatites from the absolute paleotectonic reconstructions, *Journal of Geodynamics* (2019), https://doi.org/10.1016/j.jog.2019.01.017

Geodynamic origin of carbonatites from the absolute paleotectonic reconstructions

Liya N. Kogarko[a], Roman V. Veselovskiy[b,c,*]

[a] Institute of Geochemistry RAS, Moscow, Russia

[b] Lomonosov Moscow State University, Geological Dept., Moscow, Russia

[c] Institute of Physics of the Earth RAS, Moscow, Russia

[*] Corresponding author: Roman Veselovskiy (roman.veselovskiy@ya.ru)

Graphical abstract

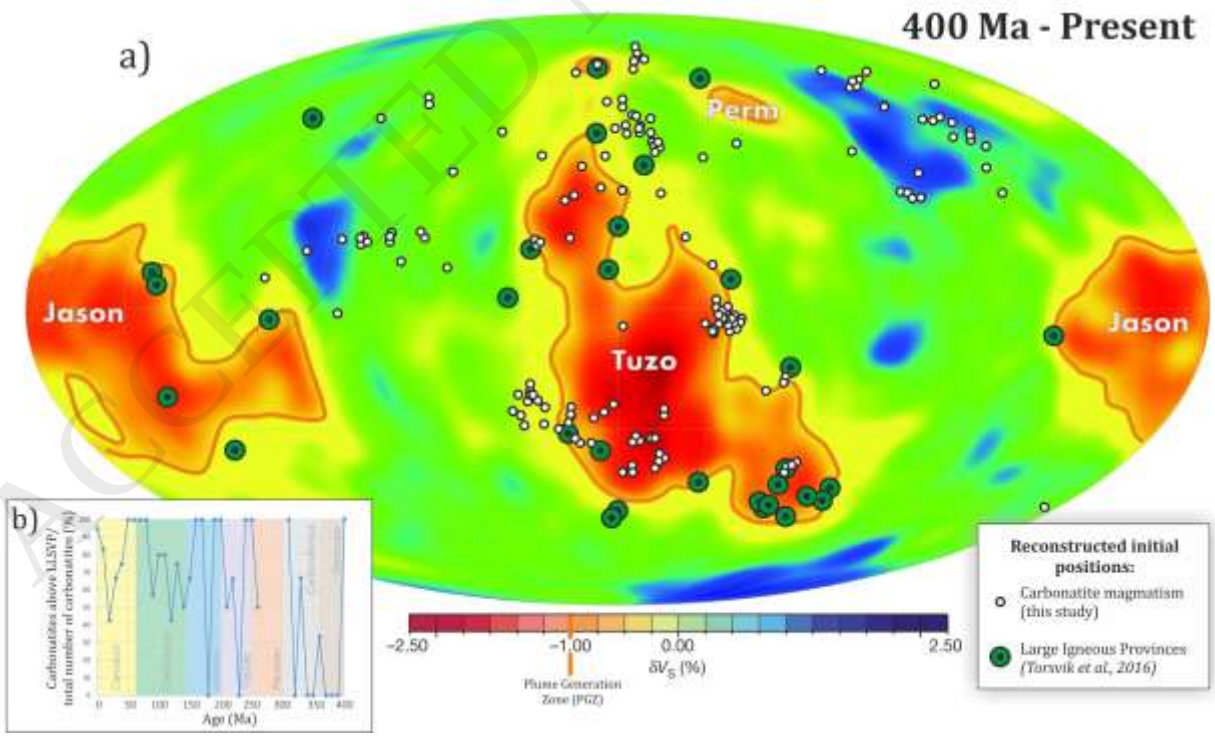

Research highlights:

- Absolute "places of birth" of 155 Phanerozoic carbonatites are reconstructed
- 69% of Phanerozoic carbonatite massifs could be linked with mantle superplumes
- 31% of carbonatites originated close to subduction graveyards in lower mantle

Abstract

Geodynamic origin of carbonatites is debated for several decades. One of hypotheses links their origin to large-volume mantle plumes rising from the core-mantle boundary (CMB). Some evidence exists for temporal and spatial relationships between the occurrences of carbonatites and large igneous provinces (LIPs), and both carbonatites and LIPs can be related to mantle plumes. A good example is the carbonatites of the Maymecha-Kotuy Province in the Polar Siberia, which were formed at the same time as the Siberian superplume event at ca. 250 Ma. In this study we use a recently published absolute plate kinematic modelling to reconstruct the position of 155 Phanerozoic carbonatites at the time of their emplacement. We demonstrate that 69% of carbonatites may be projected onto the central or peripheral parts of the large low shear-wave velocity provinces (LLSVPs) in the lowermost mantle. This correlation provides a strong evidence for the link between the carbonatite genesis and the locations of deep-mantle plumes. A large group of carbonatites (31%) has no obvious links to LLSVPs and, on the contrary, they plot above the "faster-than-average S-wave" zones in the deep mantle, currently located beneath North and Central America and China. We propose that their origin may be associated with remnants of subducted slabs in the mantle.

Keywords: carbonatites; Phanerozoic; absolute plate reconstructions; superplume; Large Igneous Provinces.

1. Introduction

Carbonatites make up only several percent of alkaline igneous rocks, but they are of a great economic importance because carbonatite rocks contain large deposits of the critical metals such as niobium and rare earth elements (REE). Currently, the entire international market of niobium and REE is supplied from the large carbonatite deposits like Bayan Obo, Mouniuping (China), Araxa (Brazil), Mountain Pass (USA) and many others (Smith at al., 2016). The analysis of the existing databases (Kogarko et al., 1995; Woolley and Kjarsgaard, 2008; Frolov et al., 2003) shows that the vast majority of carbonatites are located on continents, and they are spatially confined to ancient cratons. Only a small number of carbonatites occurs on oceanic islands, i. e. Canary Islands, Cape Verde, and Kerguelen (Woolley and Kjarsgaard, 2008).

Geodynamic settings of carbonatite formation are still actively discussed in the literature. Some researchers correlate carbonatite events with orogenic activities. For example, Gittins (1989) and Woolley (1989) have pointed out a possible relationship between carbonatite magmatism and orogenic activity in Eastern Canada and in Pakistan. Recent data indicate that carbonatites in the Southernmost Qinling province (China) belong to the Himalayan orogenic belt, and they were formed during the inter-continental collision (Song et al., 2016). Bailey (1977) underlined the lithospheric character of carbonatite emplacements in East and Central Africa, and he also proposed that the carbonatite origin was controlled by the rejuvenated deep structures in the

lithospheric mantle. Numerous carbonatites are also closely related to the rift zones, i. e. East African Province, Rhein graben etc.

Carbonatites have been considered by some researchers as having a close connection with large volumes of deep mantle material rising from the core-mantle boundary (CMB) (Ernst and Bell, 2010). Indeed, the association of carbonatites with the large igneous provinces (LIPs) has been observed, the latter being linked to the episodes of mantle plume activities (Ernst, 2014). Carbonatites are also well represented in the major provinces: Cretaceous Parana-Etendeka, Jurassic Karoo-Ferrar, Cretaceous-Paleogene Deccan and others. Nevertheless, it should be noted, that not all large magmatic events are associated with carbonatites and alkaline magmatism. In general, isotopic characteristics of carbonatites (Nelson et al., 1988; Kramm, 1993; Bell, 2001; Kogarko and Zartman, 2007; Rukhlov et al., 2015) are in a close range as basalts of oceanic islands (OIB), which are associated with mantle plume activity. Noble gas isotopic data of carbonatites also confirm their relationship to the deep-mantle reservoirs (Tolstikhin et al., 2002). Carbonatites associated with lower mantle periclase, were found as inclusions in diamonds, and this may also serve as a direct proof of carbonatite sources coming from the lowermost mantle (Kaminsky et al., 2015b).

However, the experimental data on equilibria of carbonatites with CO_2 at high temperatures and pressures corresponding to the conditions of the deepest lower mantle are ambiguous. Mathematical modeling of reactions involving carbon (Kaminsky et al., 2015a) and experimental studies (Dasgupta and Hirschman, 2006) do not support the formation of equilibrium carbonate melts at great depths due to a very low oxygen fugacity in the deep lower mantle. At the same time, the quantitative modeling of the partial melting of a material rising from the deep mantle containing an elevated CO_2 concentration (Collerson et al., 2010), as well as experimental works

on the phase equilibria of carbonates at lower mantle conditions (Dalou et al., 2009; Walter et al., 2008), clearly demonstrated the possibility of the carbonatite formation at depths corresponding to the conditions of the lowest mantle.

The presence of metasomatised and carbonated zones in the lithospheric mantle is one of the problems for adopting a model that links the carbonatite origin with deep mantle plume sources. According to a large number of publications, the metasomatism is ubiquitous in the continental and oceanic lithosphere (Ionov, 1998; Kogarko et al., 2007). On this basis it has been hypothesized that the carbonatite melts are due to the partial melting of the carbonated lithosphere. We adopt here a model that the rise of deep-mantle plumes causes partial melting at depths of approximately 200-300 km. This releases melts/fluids containing large amounts of volatile components, mainly of CO_2 and H_2O, typical for a very small degree of partial melting. They appear to be the main agents of the carbonate metasomatism in the lithospheric mantle.

The main goal of the present article is to test a regular distribution pattern of the Phanerozoic carbonatite magmatism manifestations in relation to the largest seismic velocity anomalies in the lower mantle (LLSVPs, large low-shear-wave velocity provinces), which are currently interpreted as a main source of the deep mantle plumes (Garnero et al., 2016).

2. Study Objectives and Methods

It is well known that the structure of the lowermost mantle is heterogeneous, which is reflected in the variable thickness observed for the D” layer (up to 500-600 km in thickness) and currently referred to as Large Low-Shear-Wave Velocity Provinces (LLSVPs). Many scientists believe that these structures play an important role in global geodynamics (Garnero et al., 2016)

and could be responsible for episodes of a true polar wander, for plate assembling and breakup of supercontinents (Torsvik et al., 2016), affecting activity of the geodynamo and etc. Moreover, Kuzmin et al. (2011) demonstrated that the evolution of the Siberian "within-plate" magmatism that occurred at the Paleozoic-Mesozoic boundary, could be correlated with the processes in the LLSVPs.

According to Torsvik et al. (2010, 2014, and references therein), there are several LLSVPs in the lowest mantle. The two best known are also the largest ones: one is located beneath Africa and is called "Tuzo", and the other one is beneath the Western part of Pacific Ocean, called "Jason". These two LLSVPs reach 8-10 thousand kilometers in diameter and are located in the equatorial plane, they are almost symmetrical to the Earth's mass center. The third LLSVP is much smaller; its projection falls on the European part of Russia, and it is called "Perm". The attenuation of S-waves in LLSVPs reaches up to 3% and is explained by the increased internal temperature within LLSVP relative to the surrounding mantle (Torsvik et al., 2010).

Torsvik et al. (2010) have demonstrated that there is a spatial correlation between the modern and reconstructed locations of the LIPs and of kimberlites by using the contour line of 1% S-wave attenuation (Fig. 1). This contour line corresponds to the highest temperature gradient between LLSVP and the surrounding mantle. It was called the plume generation zone (PGZ). Recently, using an assumption about the long-term stability of LLSVPs relative to the ambient mantle, the absolute plate kinematic model for the entire Phanerozoic has been developed (Domeier and Torsvik, 2014). According to this model, approximately 80% of LIPs and kimberlites are located above the PGZs.

We have now added the age-corrected position of the carbonatite localities to this model (Fig. 1). They include 155 episodes from the late Paleozoic (400 Ma) to the present-day of

carbonatite magmatism manifestations taken from all over the world modified compilation provided in Woolley and Kjarsgaard (2008; Table 1). Few carbonatites were deleted from the original database because of their uncertain tectonic settings, and the ages of some carbonatite massifs were corrected according to the new geochronological data (Table 1, see footnote). The number of carbonatites is limited by the Early-Middle Devonian boundary (400 Ma), i. e. by the time limit of the kinematic model (Matthews et al., 2016). The paleotectonic reconstructions are drawn with 10 Myr steps because the changes in the plate positions are insignificant when a smaller time interval is used, and, therefore, it has no influence on the final results. Accordingly, all the carbonatites were dated using the 10 Myr averaging gliding window (Table 1, see Reconstruction Age column). For example, all the carbonatites having ages 0-5 Ma are reconstructed in the present tectonic pattern; the carbonatites with the ages belonging to 5-15 Ma interval are reconstructed in the 10 Ma pattern, etc.

This model uses the newest absolute plate kinematic modelling (Matthews et al., 2016) and GPlates 2.0 software (Williams et al., 2012) to reconstruct the initial position of carbonatites in the past. The carbonatite massifs were considered to be linked with the LLSVPs, if their reconstructed locations were not more than 10° (~1110 km) away from a LLSVP boundary (i.e. the borderline between yellow and green colors in Fig. 1).

3. Discussion

3.1 Carbonatites above LLSVPs

Using selected carbonatite massifs (Table 1) and the absolute plate kinematic model (Matthews et al., 2016), the positions of the carbonatite occurrences for the last 400 Myr were reconstructed in coordination with the projection of the LLSVPs onto the Earth's surface (Fig. 1;

see Supplementary). The analysis of these reconstructions allows us to conclude that 69% (107 of 155) of all observed carbonatites are projected onto central or peripheral areas of the LLSVPs. Most of these carbonatite projections are located above or are close to the African LLSVP "Tuzo" with a tail stretched out beneath Iceland. Very few carbonatites lie close to the small "Perm" LLSVP, and only one massif is linked to the Pacific "Jason" LLSVP. This distribution pattern can be viewed as a strong evidence for the mantle plume origin of these groups of carbonatites. The almost absence of carbonatites occurring above the Pacific LLSVP ("Jason") is a striking illustration of the importance of a thicker and older continental lithosphere for the appearance and development of carbonatites. The specific locality distribution also confirms the permanent presence of oceanic lithosphere in this part of the Earth (at least during the last 400 Myr), where carbonatite occurrences were quite rare.

The comparison of in Fig. 1 reconstructions with in Torsvik et al. (2010) Fig. 1 leads to the conclusion that the reconstructed positions of carbonatites, LIPs and kimberlites coincide with the locality of the African LLSVP. This could be a result of the genetic similarity of these magmatic types of rocks, but it should be also noted here that kimberlites being distinct from carbonatites, do not appear above the increased ("faster-than-average") S-wave anomalies in the lowermost mantle, as it is the case of the Chinese carbonatites (Fig. 1; see Supplementary). The same is true for LIPs, which are mainly projected on the edges of the LLSVPs. These features are apparently related to some differences in the physicochemical conditions of these rock formations.

The Maymecha-Kotuy Province is located in the northern part of Siberian Platform (Polar Siberia) along the NE margin of Siberian Traps, which is one of the world's largest ultramafic-alkaline-carbonatite associations. The province comprises a large volume of alkaline-ultramafic lavas and hundreds of dykes as well as several carbonatite bodies (for instance, Odikhincha,

Kugda, and Dolbykha), and also more than 30 separate intrusive bodies, including the world's largest ultramafic-alkaline-carbonatite complex, the Guli pluton. The ages and Pb, Sr, and Nd isotopic systematics of the Siberian flood basalts and the Guli ultramafic alkaline-carbonatite association (Kogarko and Zartman, 2007) demonstrate the formation of the Siberian traps (249±2 Ma,) contemporaneous with the Polar Siberian carbonatites (250±9 Ma), as well as their genetic link (Dalrymple et al., 1995). According to the new data, the age of carbonatites of Odikhincha and Kugda massifs is 250±2 Ma (Kogarko and Lebedev, in press).

At the Cretaceous-Paleogene boundary, the large volume of tholeiitic basalts and alkaline-carbonatite rocks were emplaced in the Deccan plateau in India. The tectonic development of the Deccan LIP is resulted from its separation from the Seychelles microcontinent. The overlap of ages between carbonatites (67 Ma, Amba-Dongar, Mundwara) and Deccan flood basalts (67.5 Ma) is very likely a result of the direct plume-carbonatite linking.

The Paraná-Etendeka flood basalts (138-128 Ma) make up a large igneous province, which includes both the main Paraná traps (in Paraná Basin, South America) and the smaller traps at Etendeka (in northwest Namibia and southwest Angola). These events have been associated with the thermal and/or chemical influence of the mantle-plumes impacting the base of the continental lithosphere, resulting in the break-up of Gondwana supercontinent (Gibson et al., 1995; Carlson et al., 1996; Thompson et al., 1998). The alkaline-carbonatite magmatism of the same age is associated with the Paraná (Cerro Chiriguelo, Cerro Guazu, Cerro Sarambi, Serra Negra, Salitre, Araxá, Tapira) and Etendeka (Okenyenya, Okorusu and Ondurakorume complexes) provinces (Milner et al., 1995). The correlation between the tectonic and magmatic evolution of Parana-

Etendeka in South America and South Africa convincingly demonstrates the genetic link of the alkaline-carbonatite magmatism and a mantle plume activity.

3.2 Carbonatites not lying above a LLSVP

As it is inferred from the aforementioned reconstructions (Fig. 1; see Supplementary), a significant proportion (31%; 48 out of 155) of the Phanerozoic carbonatites are located far away from a LLSVP at the time of their emplacement, for instance, from China and Kola Peninsula. Most of them are located above, or close to the two zones in the lowermost mantle with the "faster-than-average" S-wave velocities. There are two potential reasons for this: (1) the limitation of the plate kinematic model used in this study, or (2) the differences in geodynamic settings for these carbonatites, which may have no connection with LLSVPs. Both of these possibilities are discussed below.

The strangest result inferred from the tectonic reconstructions is that the Devonian-age Kola alkaline province does not lie above a LLSVP. The Kola Province is one of the largest alkaline-carbonatite associations, with more than 30 massifs and the world's two largest layered peralkaline complexes. There are no tholeitic basalts in this province except the dyke swarms of doleritic composition. The isotopic ages of the carbonatites and alkaline rocks of the Kola Province indicate that they were emplaced in Late Devonian, at 365-370 Ma ago (Kramm and Kogarko, 1994; Arzamastsev et al., 2005, 2017). The isotopic composition of the carbonatites, alkali rocks and rare-metal ores estimated in (Kogarko et al., 2010) indicates that many of them have mantle sources with a character close to the FOZO reservoir, which may be considered as a marker of the plume magmatism (Stracke et al., 2005). These results were recently confirmed by the work on the Pb-isotopic composition of the alkaline rocks from Kola Peninsula (Zartman and Kogarko,

2017). Tolstikhin et al. (2002) concluded that the Kola Alkaline Province was likely related to a lower mantle plume with an initial $^4He/^3He$ ratio of $3 \cdot 10^4$.

Taking into account the arguments presented above, the Devonian plate reconstructions may be examined more closely. According to the recent absolute plate kinematic models (Torsvik et al., 2014; Domeier and Torsvik, 2014) that were used as a basis for the kinematic modelling in this study (Matthews et al., 2016): during the Mid-Late Devonian Baltica drifted at lower latitudes of the northern hemisphere for long distances (>4000 km) from the African and Pacific LLSVPs (see Supplementary). Torsvik et al. (2014) noted that a very limited number of paleomagnetic data for the 400-330 Ma time interval does not allow a precise reconstruction of the Siberia and Laurussia locations. In this case, the longitudinal correction of Laurussia for this time period was made only using the data from North American kimberlites having ages of 410, 390 and 370 Ma. At the same time, the presence of the Late Devonian-Early Carboniferous kimberlites on Kola Peninsula and in the Arkhangelsk region, located at a considerable distance from LLSVPs, were not explained by the kinematic model in Torsvik et al. (2014).

It is important to note here that the absolute plate kinematic models (Torsvik et al., 2014; Matthews et al., 2016) and "classical", non-longitudinally corrected paleotectonic reconstructions (Scotese, 2016), constrain significantly the relative positions of Laurussia and surrounding landmasses such as Siberia and Gondwana during the Devonian and Carboniferous. The most noticeable and meaningful discrepancy occurs in the 370-320 Ma time interval, when according to the kinematic model, Laurussia moved fast approximately 6000 km eastward with an average velocity of ~10 cm/year. The reasons for this drift were explained above: Laurussia is literally attached to the eastern edge of the Pacific LLSVP ("Jason") by its kimberlite localities, and as soon as kimberlite magmatism ceases ca. 370 Ma, then Laurussia immediately rushes eastwards

on order to be on time (~320-310 Ma) for its "classical" position within the Pangaea supercontinent. In the absence of any obvious arguments (apart from North American kimberlites) for the Laurussia's drift and following the plate movement minimization principle, we have used the "classical" position of Laurussia for 390-310 Ma reconstructions, as suggested by Scotese (2016), see Fig. 2. In this case, all the Kola's carbonatites are located above the African LLSVP at the time of their emplacement, which is consistent with the arguments of their lower mantle source. However, a question remains about the origin of the North American 360-320 Ma carbonatites (and kimberlites) which are located far away from a LLSVP. Thus, the use of two alternative tectonic reconstruction models does not solve the problem of the geodynamic positions of the Kola or North American Devonian-Carboniferous kimberlites and carbonatites.

Another possible explanation for the concentration of carbonatites above the lowermost mantle regions with "faster-than-average" S-wave velocities is that they have different geodynamic origins. Torsvik et al. (2016) noted the presence of kimberlites originating above two (or one large) "faster-than-average lower mantle" regions, which are project onto present-day North and Central America. However, no kimberlites are emplaced above the analog areas beneath Asia. Another situation is observed with the carbonatites concentrated above or close to the both of these anomalous zones. Many researchers consider the "faster-than-average" zones as a location of descending cold mantle flows, thermally dominated by the subducted slab material (Torsvik et al., 2016). If it is so, the origin of the mentioned carbonatites could be linked to deeply carbon-bearing subducted slabs, as it has been suggested by Walter et al. (2008). One of the possible mechanisms for the generation of carbonatite magmas might be associated with a heat flow increase after formation of a thick large landmass, such as supercontinent, which does not require the presence of a mantle plume. As it was shown by (Coltice et al., 2007), the reorganization of a

convective flow after the continental assembly can be responsible for a positive temperature excursion up to 100°C or more. Such a large-scale thermal anomaly would be sufficient to trigger a partial melting within the subcontinental mantle and to move carbonatite melts upward into the crust. This effect would be of a greater importance especially, if the lithospheric mantle were hydrated during a recent subduction. Taking into account the physical and thermal properties of carbonatite magmas, such as low viscosity and low heat of fusion (Treiman and Schedl, 1983), the emplacement time and the thermal effect of such an emplacement could be significant. Similar "non-plume" models of basalt provinces formation have been recently suggested and discussed in details in (Ivanov, 2007), so we cannot exclude these scenarios of the carbonatite origin, to explain why they are located far away from LLSVPs.

From other point of view, some carbonatites can be associated with active orogenic events: the Quinling orogen carbonatite province (China) might be a good example of such connection (Song et al., 2016).

Moreover, according to Kellogg et al. (1999) the volume of ancient recycled and subducted materials is approximately 20-30% of the lower mantle volume. This long-lived geochemical reservoir likely has a higher oxygen potential and recycled carbon, which would facilitate a carbonatite formation. Notably, a similar genetic model was recently suggested for the Yellowstone Volcanic Province (Zhou et al., 2018).

4. Conclusions

The indicated above carbonatite magmatism manifestations in the system of the global absolute paleotectonic reconstructions (Matthews et al., 2016) reveal that 69% of them could be linked with the large low-shear-wave velocity provinces (LLSVPs) in the lowest mantle, currently

interpreted to be linked to the deep mantle superplumes. This conclusion could be considered as a decisive argument for deep mantle sources of the carbonatite magmatism on the Earth. At the same time, it has been shown that approximately 31% of carbonatites were formed far away from the LLSVPs, and many of them (33 of 48) spatially correlate with the "faster-than-average" S-wave zones beneath North and Central America and Asia. Using of the alternative plate reconstruction model of (Scotese, 2016) for Devonian time makes possible to associate an origin of the Kola Devonian carbonatite massifs with the African LLSVP, but this pattern does not explain the origin of the North American 360-320 Ma age carbonatites and kimberlites. The carbonatites above the "faster-than-average" S-wave zones could be genetically connected with the ancient carbon-bearing subducted material in the upper or even lower mantle, the thermal and density effects of which could be a consequence of the physical properties of carbonatite melts.

Acknowledgments

We are grateful to G. Brey, N. Bagdasarov, F. Woodland, F. Kaminsky and two reviewers, N. Arndt and W. Griffin for many helpful comments and suggestions. This work was supported by the Russian Academy of Sciences grant 2018-0039, I.48P, Scientific, the grant of President of the Russian Federation (MD1116.2018.5) and by Russian Foundation for Basic Research (grant #18-35-20058).

References

Arzamastsev, A.A., Belyatsky, B. V., Travin, A. V., Arzamastseva, L. V., Tsarev, S.E., 2005. Dike rocks in the Khibina Massif: Relations with the plutonic series, age, and characteristics of the mantle source. Petrology 13(3), 267–288.

Arzamastsev, A.A., Veselovskiy, R. V., Travin, A. V., Yudin, D.S., Belyatsky, B. V., 2017. Paleozoic tholeiitic magmatism of the Kola province: Spatial distribution, age, and relation to alkaline magmatism. Petrology. https://doi.org/10.1134/S0869591116060023

Bailey, D.K., 1977. Lithosphere control of continental rift magmatism. Geological Society of London Journal 133, 103-106. https://doi.org/10.1144/gsjgs.133.1.0103

Bell, K., 2001. Carbonatites: relationships to mantle-plume activity. In: Ernst RE, Buchan KL (eds) Mantle plumes: their identification through time. Geological Society of America, Special Paper 352, 267–290.

Carlson, R.W., Esperanca, S., Svisero, D.P., 1996. Chemical and Os isotopic study of Cretaceous potassic rocks from Southern Brazil. Contributions to Mineralogy and Petrology 125(4), 393–405. https://doi.org/10.1007/s004100050230.

Collerson, K.D., Williams, Q., Ewart, A.E., Murphy, D.T., 2010. Origin of HIMU and EM-1 domains sampled by ocean island basalts, kimberlites and carbonatites: The role of CO_2-fluxed lower mantle melting in thermochemical upwellings. Physics of the Earth and Planetary Interiors 181 (3–4), 112–131. https://doi.org/10.1016/j.pepi.2010.05.008.

Comin-Charmant, P., Gomes, C.B., 2005. Mesozoic to Cenozoic alkaline magmatism of Brazilian Platform. Sao Paulo. FAPESP. 752 p.

Coltice, N., Phillips, B.R., Bertrand, H., Ricard, Y., Rey, P., 2007. Global warming of the mantle at the origin of flood basalts over supercontinents. Geology. https://doi.org/10.1130/G23240A.1

Dalou, C., Koga, K.T., Hammouda, T., Poitrasson, F., 2009. Trace element partitioning between carbonatitic melts and mantle transition zone minerals: Implications for the source of carbonatites. Geochimica et Cosmochimica Acta 73(1), 239–255. https://doi.org/10.1016/j.gca.2008.09.020

Dalrymple, G.B., Czamanske, G.K., Fedorenko, V.A., Simonov, O.N., Lanphere, M.A., Likhachev, A.P., 1995. A reconnaissance $^{40}Ar/^{39}Ar$ geochronologic study of ore-bearing and related rocks, Siberian Russia. Geochim. Cosmochim. Acta. https://doi.org/10.1016/0016-7037(95)00127-1

Dasgupta, R., Hirschmann, M.M., 2006. Melting in the Earth's deep upper mantle caused by carbon dioxide. Nature. https://doi.org/10.1038/nature04612

Domeier, M., Torsvik, T.H., 2014. Plate tectonics in the late Paleozoic. Geosci. Front. https://doi.org/10.1016/j.gsf.2014.01.002

Ernst, R.E., Bell, K., 2010. Large igneous provinces (LIPs) and carbonatites. Mineralogy and Petrology 98(1–2), 55–76. https://doi.org/10.1007/s00710-009-0074-1

Ernst, R.E., 2014. Large Igneous Provinces. Cambridge University Press, 666 p.

Garnero, E.J., McNamara, A.K., Shim, S.H., 2016. Continent-sized anomalous zones with low seismic velocity at the base of Earth's mantle. Nature Geoscience 9, no. 7, 481-489. https://doi.org/10.1038/ngeo2733.

Gibson, S.A., Thompson, R.N., Leonardos, O.H., Dickin, A.P., Mitchell, J.G., 1995. The late cretaceous impact of the Trindade mantle plume: Evidence from large-volume, mafic,

potassic magmatism in SE Brazil. Journal of Petrology 36(1), 189–229. https://doi.org/10.1093/petrology/36.1.189.

Gittins, J., 1989. The origin and evolution of carbonatite magmas, in: Bell K. (Ed.), Carbonatites: genesis and evolution. Unwin Hyman, London, United Kingdom, 618 p.

Frolov, A.A., Tolstov, A.V., Belov, S.V., 2003. Carbonatite Deposits of Russia. NIA-Priroda, Moscow, pp. 494 (in Russian).

Ionov, D., 1998. Trace Element Composition of Mantle-derived Carbonates and Coexisting Phases in Peridotite Xenoliths from Alkali Basalts. Journal of Petrology 39(11–12), 1931–1941. https://doi.org/10.1093/petroj/39.11-12.1931.

Ivanov, A. V., 2007. Evaluation of different models for the origin of the Siberian Traps, in: Special Paper 430: Plates, Plumes and Planetary Processes. https://doi.org/10.1130/2007.2430(31)

Kaminsky, F.V., Ryabchikov, I.D., Wirth, R., 2015a. A primary natrocarbonatitic association in the Deep Earth. Mineralogy and Petrology 110, 2, 387-398. DOI 10.1007/s00710-00015-00368-00714

Kaminsky, F. V., Ryabchikov, I.D., McCammon, C.A., Longo, M., Abakumov, A.M., Turner, S., Heidari, H., 2015b. Oxidation potential in the Earth's lower mantle as recorded by ferropericlase inclusions in diamond. Earth Planet. Sci. Lett. https://doi.org/10.1016/j.epsl.2015.02.029

Kamo, S.L., Czamanske, G.K., Amelin, Y., Fedorenko, V.A., Davis, D.W., Trofimov, V.R., 2003. Rapid eruption of Siberian flood-volcanic rocks and evidence for coincidence with the Permian-Triassic boundary and mass extinction at 251 Ma. Earth Planet. Sci. Lett. https://doi.org/10.1016/S0012-821X(03)00347-9

Kellogg, L.H., Hager, B.H., van der Hilst, R.D., 1999. Compositional stratification in the deep mantle. Science 283(5409), 1881–1884. https://doi.org/10.1126/science.283.5409.1881

Kogarko, L.N., Kononova, V.A., Orlova, P., Woolley, A.R., 1995. Alkaline Rocks and Carbonatites of the World. Part Two: Former USSR. March, Chapman & Hall, 224 p.

Kogarko, L.N., Kurat, G., Ntaflos, T., 2007. Henrymeyerite in the metasomatized upper mantle of eastern Antarctica. Canadian Mineralogist 45(3), 497–501. https://doi.org/10.2113/gscanmin.45.3.497

Kogarko, L.N., Zartman, R.E., 2007. A Pb isotope investigation of the Guli massif, Maymecha-Kotuy alkaline-ultramafic complex, Siberian flood basalt province, Polar Siberia. Mineralogy and Petrology 89(1–2), 113–132. https://doi.org/10.1007/s00710-006-0139-3

Kogarko, L.N., Lahaye, Y., Brey, G.P., 2010. Plume-related mantle source of super-large rare metal deposits from the Lovozero and Khibina massifs on the Kola Peninsula, Eastern part of Baltic Shield: Sr, Nd and Hf isotope systematics. Mineralogy and Petrology 98(1–2), 197–208. https://doi.org/10.1007/s00710-009-0066-1

Kramm, U., 1993. Mantle components of carbonatites from the Kola Alkaline Province, Russia and Finland: A Nd - Sr study. Eur. J. Mineral. 5. 985-989.

Kramm, U., Kogarko, L.N., 1994. Nd and Sr isotope signatures of the Khibina and Lovozero agpaitic centres, Kola Alkaline province, Russia. Lithos 32(3–4), 225–242. https://doi.org/10.1016/0024-4937(94)90041-8

Kuzmin, M.I., Yarmolyuk, V.V., Kravchinsky, V.A., 2011. Phanerozoic Within-Plate Magmatism of North Asia: Absolute Paleogeographic Reconstructions of the African Large Low-Shear-Velocity Province. Geotectonics, 45 (6), 415–438.

Matthews, K.J., Maloney, K.T., Zahirovic, S., Williams, S.E., Seton, M., Müller, R.D., 2016. Global plate boundary evolution and kinematics since the late Paleozoic. Global and Planetary Change 146, 226–250. https://doi.org/10.1016/j.gloplacha.2016.10.002

Milner, S.C., Duncan, A.R., Whittingham, A.M., Ewart, A., 1995. Trans-Atlantic correlation of eruptive sequences and individual silicic volcanic units within the Paraná-Etendeka igneous province. Jour. Volcanol. Geotherm. Res. https://doi.org/10.1016/0377-0273(95)00040-2

Nelson, D.R., Chivas, A.R., Chappell, B.W., McCulloch, M.T., 1988. Geochemical and isotopic systematics in carbonatites and implications for the evolution of ocean-island sources. Geochim. Cosmochim. Acta. https://doi.org/10.1016/0016-7037(88)90051-8

Rukhlov, A.S., Bell, K., 2010. Geochronology of carbonatites from the Canadian and Baltic shields, and the Canadian Cordillera: Clues to mantle evolution. Mineralogy and Petrology 98(1–2), 11–54. https://doi.org/10.1007/s00710-009-0054-5

Rukhlov, A., Bell, K., Amelin, Y., 2015. Symposium on critical and strategic materials. British Columbia Geological Survey Paper, 39-64.

Song, WL; Xu, C; Smith, M.P; Kynicky, J; Huang, KJ; Wei, CW; Zhou, L; Shu, QH, 2016. Origin of unusual HREE-Mo-rich carbonatites in the Qinling orogen, China. Scientific Reports 6, doi: 10.1038/srep37377

Scotese, C.R., 2016. PALEOMAP PaleoAtlas for GPlates and the PaleoData Plotter Program, PALEOMAP Project, http://www.earthbyte.org/paleomap-paleoatlas-for-gplates/

Smith, E.M., Shirey, S.B., Nestola, F., Bullock, E.S., Wang, J., Richardson, S.H., Wang, W., 2016. Large gem diamonds from metallic liquid in Earth's deep mantle. Science 354. https://doi.org/10.1126/science.aal1303

Stracke, A., Hofmann, A.W., Hart, S.R., 2005. FOZO, HIMU, and the rest of the mantle zoo. Geochemistry, Geophys. Geosystems. https://doi.org/10.1029/2004GC000824

Thompson, R.N., Gibson, S.A., Mitghell, J.G., Dickin, A.P., Leonardos, O.H., Brod, J.A., Greenwood, J.G., 1998. Migrating Cretaceous-Eocene magmatism in the Serra do Mar Alkaline Province, SE Brazil: melts from the deflected Trindade mantle plume? Journal of Petrology 39(8), 1493–1526. https://doi.org/10.1093/petroj/39.8.1493

Tolstikhin, I.N., Kamensky, I.L., Marty, B., Nivin, V.A., Vetrin, V.R., Balaganskaya, E.G., Ikorsky, S. V., Gannibal, M.A., Weiss, D., Verhulst, A., Demaiffe, D., 2002. Rare gas isotopes and parent trace elements in ultrabasic-alkaline-carbonatite complexes, Kola Peninsula: Identification of lower mantle plume component. Geochim. Cosmochim. Acta. https://doi.org/10.1016/S0016-7037(01)00807-9

Torsvik, T.H., Burke, K., Steinberger, B., Webb, S.J., Ashwal, L.D., 2010. Diamonds sampled by plumes from the core-mantle boundary. Nature. https://doi.org/10.1038/nature09216

Torsvik, T.H., Steinberger, B., Ashwal, L.D., Doubrovine, P. V., Trønnes, R.G., 2016. Earth evolution and dynamics – a tribute to Kevin Burke. Can. J. Earth Sci. https://doi.org/10.1139/cjes-2015-0228

Torsvik, T.H., van der Voo, R., Doubrovine, P.V., Burke, K., Steinberger, B., Ashwal, L.D., Bull, A.L., 2014. Deep mantle structure as a reference frame for movements in and on the Earth. Proceedings of the National Academy of Sciences USA 111, 8735–8740. https://doi.org/10.1073/pnas.1318135111.

Treiman, A.H., Schedl, A., 1983. Properties of Carbonatite Magma and Processes in Carbonatite Magma Chambers. J. Geol. https://doi.org/10.1086/628789

Walter, M.J., Bulanova, G.P., Armstrong, L.S., Keshav, S., Blundy, J.D., Gudfinnsson, G., Lord, O.T., Lennie, A.R., Clark, S.M., Smith, C.B., Gobbo, L., 2008. Primary carbonatite melt from deeply subducted oceanic crust. Nature. https://doi.org/10.1038/nature07132

Williams, S.E., Dietmar Müller, R., Landgrebe, T.C.W., Whittaker, J.M., 2012. An open-source software environment for visualizing and refining plate tectonic reconstructions using high-resolution geological and geophysical data sets. GSA Today. https://doi.org/10.1130/GSATG139A.1

Woolley, A.R, 1989. The spatial and temporal distribution of carbonatites, in: Bell K. (Ed.), Carbonatites: genesis and evolution. Unwin Hyman, London, United Kingdom, 618 p.

Woolley, A.R., Kjarsgaard, B.A., 2008. Carbonatite occurrences of the world: map and database. Geological Survey of Canada, Open File 5796, 1 CD-ROM plus 1 map.

Zartman, R.E., Kogarko, L.N., 2017. Lead isotopic evidence for interaction between plume and lower crust during emplacement of peralkaline Lovozero rocks and related rare-metal deposits, East Fennoscandia, Kola Peninsula, Russia. Contributions to Mineralogy and Petrology, 172(32). https://doi.org/10.1007/s00410-017-1348-y.

Zhou, Q., Liu, L., Hu, J., 2018. Western US volcanism due to intruding oceanic mantle driven by ancient Farallon slabs. Nat. Geosci. https://doi.org/10.1038/s41561-017-0035-y

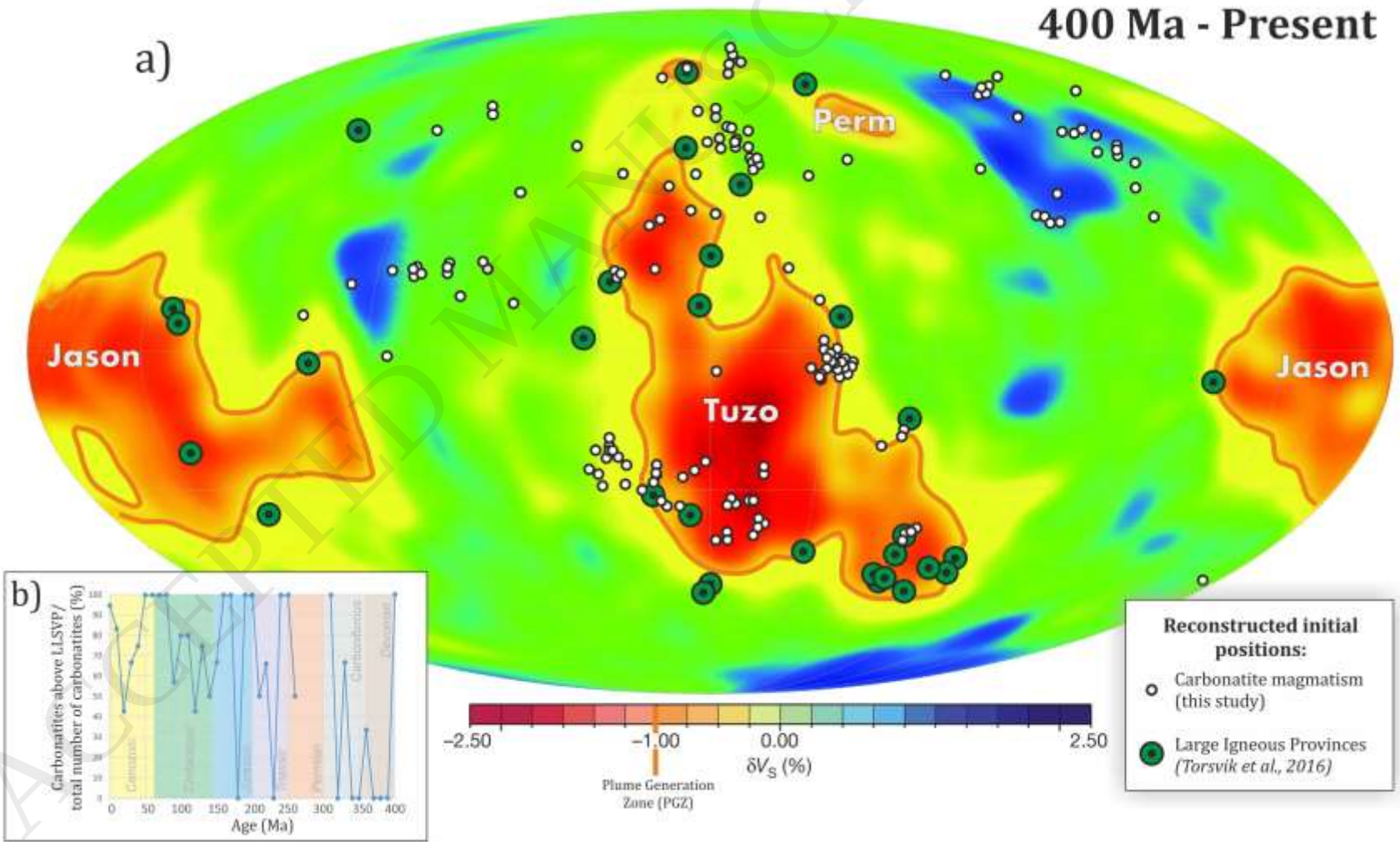

Figure 1. (a) Absolute reconstructed localities of the present to the late Paleozoic (0-400 Ma) carbonatites according to the recent plate reconstruction model from (Matthews et al., 2016). The color corresponds to the rate of change of S-wave according to the tomographic SMEAN lower mantle at a depth of 2800 km (Becker and Boschi, 2002). The figure also shows the outline of 1% -s' velocity S-wave

abnormality, which is considered by many researchers as the main area of generation of mantle plumes. (b) Ratio of the number of carbonatites formed above the LLSVPs to the total number of carbonatites manifestations during the period of 10 Myr.

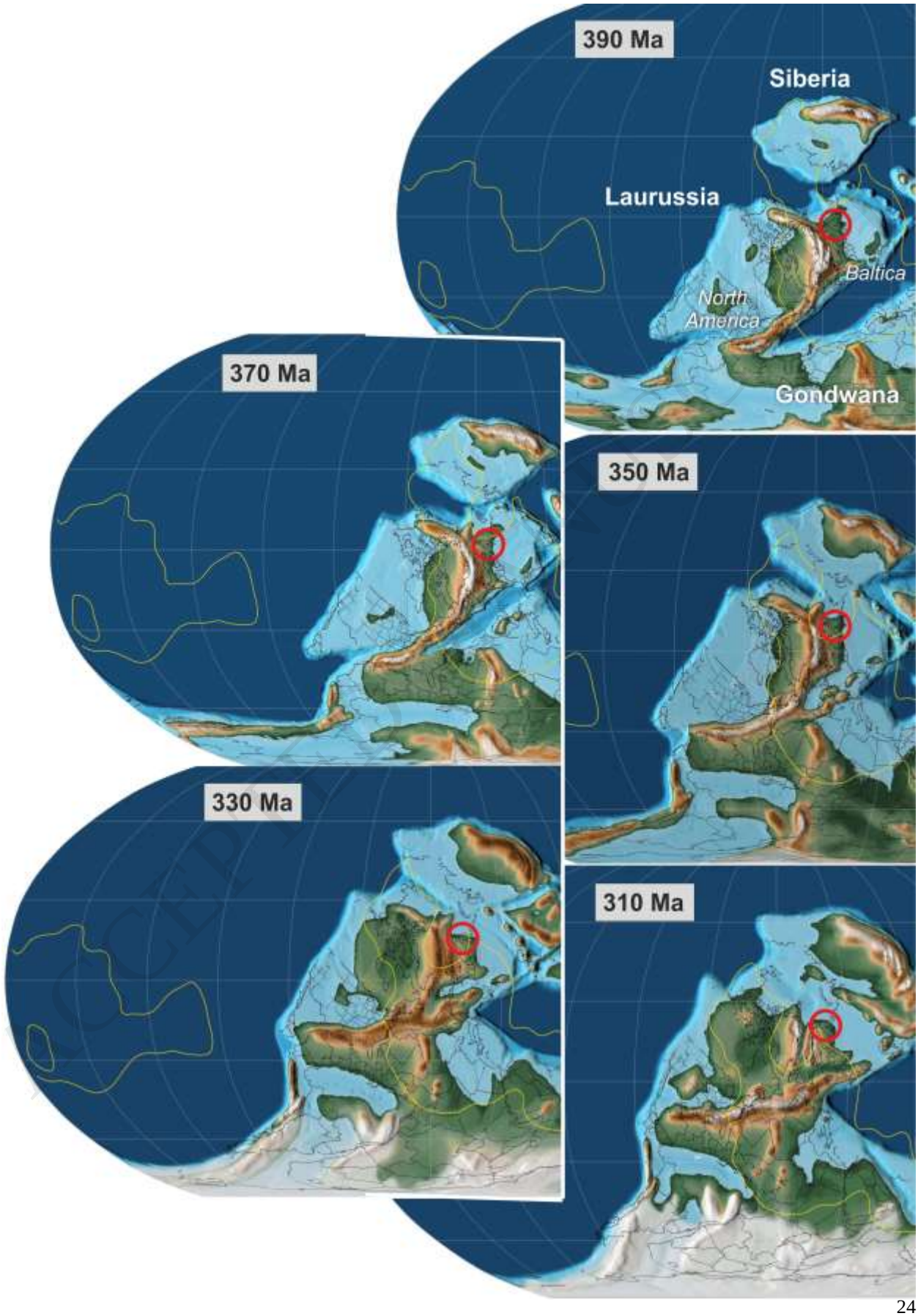

Figure 2. Alternative paleotectonic reconstructions of relative locations for Laurussia, Siberia and Gondwana in Devonian and Carboniferous (Scotese, 2016). Yellow line marks PGZ contour. Red circle pointed the Kola Devonian Alkaline province position.

Table 1. The list of carbonatites used in paleotectonic reconstructions. After Woolley and Kjarsgaard (2008) with minor changes.

NN	ID Number	Lat (°)	Long (°)	Age (Ma)	Locality	Country	Continent	Reconstruction Age (Ma)	Plate ID
1	497	50.400	7.183	0	Laacher See	Germany	Europe	0	301
2	126	-2.767	35.917	0	Oldoinyo Lengai	Tanzania	Africa	0	701
3	146	0.683	30.250	0	Fort Portal and Kasekere	Uganda	Africa	0	701
4	505	40.967	15.633	0.1	Monticchio	Italy	Europe	0	307
5	502	42.600	12.850	0.2	Polino	Italy	Europe	0	307
6	501	42.867	12.267	0.3	San Venanzo	Italy	Europe	0	307
7	148	-0.233	30.083	0.45	Bunyaruguru	Uganda	Africa	0	701
8	498	50.250	6.667	0.5	Auf Dickel	Germany	Europe	0	301
9	504	42.100	13.083	0.5	Oricola	Italy	Europe	0	307
10	127	-2.867	35.950	0.5	Kerimasi	Tanzania	Africa	0	701
11	503	42.417	12.933	0.6	Cupaello	Italy	Europe	0	307
12	132	-4.217	35.817	1.1	Kwahera	Tanzania	Africa	0	701
13	134	-4.433	35.400	1.2	Hanang and Balangida	Tanzania	Africa	0	701
14	125	-2.567	35.850	1.28	Mosonik	Tanzania	Africa	0	701
15	523	14.867	-24.700	1.4	Brava	Cape Verdes	Oceanic Islands	0	701

NN	ID Number	Lat (°)	Long (°)	Age (Ma)	Locality	Country	Continent	Reconstruction Age (Ma)	Plate ID
16	36	-2.150	36.100	2	Shombole	Kenya	Africa	0	701
17	130	-3.367	36.600	2.12	Monduli-Arusha tuff cones	Tanzania	Africa	0	701
18	128	-3.183	35.417	3.91	Sadiman	Tanzania	Africa	0	701
19	524	14.917	-24.500	4.2	Fogo	Cape Verdes	Oceanic Islands	0	701
20	339	29.500	95.000	4.5	Namjagbarwa	China	Asia	0	601
21	522	16.850	-24.983	5.7	Sao Vicente	Cape Verdes	Oceanic Islands	10	701
22	512	38.900	-3.933	6	Calatrava	Spain	Europe	10	301
23	321	41.333	86.167	6.3	Yuli	China	Asia	10	601
24	33	-0.383	34.500	6.6	Homa Mountain	Kenya	Africa	10	701
25	32	-0.550	34.367	7.5	North and South Ruri	Kenya	Africa	10	701
26	525	15.100	-23.700	7.7	Sao Tiago	Cape Verdes	Oceanic Islands	10	701
27	495	44.900	4.233	8.5	Chabrieres	France	Europe	10	301
28	526	15.200	-23.167	8.9	Maio	Cape Verdes	Oceanic Islands	10	701
29	35	-0.067	35.333	12.6	Tinderet and Londiani	Kenya	Africa	10	701
30	333	33.917	104.867	13	Lixian	China	Asia	10	601
31	30	-0.483	34.383	14.3	Wasaki Peninsula	Kenya	Africa	10	701

NN	ID Number	Lat (°)	Long (°)	Age (Ma)	Locality	Country	Continent	Reconstruction Age (Ma)	Plate ID
32	31	-0.483	34.400	14.5	Nyamaji	Kenya	Africa	10	701
33	149	2.833	34.200	15.5	Toror	Uganda	Africa	20	701
34	500	47.767	8.800	15.7	Hegau	Germany	Europe	20	301
35	499	48.067	7.683	16.4	Kaiserstuhl	Germany	Europe	20	301
36	151	2.150	34.283	22.1	Napak	Uganda	Africa	20	701
37	521	28.367	-14.067	24.2	Fuerteventura, Ajui-Solapa	Canaries	Oceanic Islands	20	701
38	465	39.617	31.317	24.2	Kizilcaoren district	Turkey	Asia	20	301
39	484	-44.100	169.350	24.3	Haast River	New Zealand	Australasia	20	806
40	520	28.667	-13.983	27.5	Fuerteventura, Esquinzo	Canaries	Oceanic Islands	30	701
41	38	22.250	23.667	27.6	Unnamed	Libya	Africa	30	701
42	29	-0.567	34.150	28	Kisingiri and Rangwa	Kenya	Africa	30	701
43	486	50.683	14.183	31.1	Roztoky	Czech Republic	Europe	30	301
44	155	0.867	34.283	32.5	Bukusu	Uganda	Africa	30	701
45	340	28.833	102.000	34	Maoniuping	China	Asia	30	601
46	93	-27.933	15.717	37	Chamais	Namibia	Africa	40	701
47	156	0.683	34.183	40	Tororo	Uganda	Africa	40	701

NN	ID Number	Lat (°)	Long (°)	Age (Ma)	Locality	Country	Continent	Reconstruction Age (Ma)	Plate ID
48	64	32.567	-4.650	43	Tamazert	Morocco	Africa	40	701
49	265	44.483	-104.450	44.5	Bear Lodge Mountains	USA	America North	40	101
50	63	34.417	3.100	47	Taourirt area	Morocco	Africa	50	701
51	89	-26.467	16.017	48.9	Dicker Willem	Namibia	Africa	50	701
52	249	68.617	-33.150	50.3	Gardiner	Greenland	America North	50	101
53	119	-30.500	29.083	63.4	Melkfontein	South Africa	Africa	60	701
54	306	-24.750	-49.200	66.3	Mato Preto	Brazil	America South	70	201
55	349	24.833	72.517	67	Mundwara	India	Asia	70	501
56	356	21.983	74.067	67	Amba Dongar	India	Asia	70	501
57	299	-19.883	-46.833	69.5	Tapira	Brazil	America South	70	201
58	88	-25.867	17.833	72.5	Gross Brukkaros	Namibia	Africa	70	701
59	123	-32.483	20.850	74.6	Saltpetrekop	South Africa	Africa	70	701
60	307	-27.667	-50.250	76	Lages	Brazil	America South	80	201
61	297	-19.350	-46.100	78.2	Sao Gotardo	Brazil	America South	80	201
62	296	-19.050	-46.783	80.7	Salitre	Brazil	America South	80	201
63	295	-18.917	-46.833	81.6	Serra Negra	Brazil	America South	80	201

NN	ID Number	Lat (°)	Long (°)	Age (Ma)	Locality	Country	Continent	Reconstruction Age (Ma)	Plate ID
64	294	-18.133	-47.833	82.9	Catalao I	Brazil	America South	80	201
65	59	21.067	-11.367	85	Richat Dome	Mauritania	Africa	80	701
66	22	28.133	34.650	87	El Khafa	Egypt	Africa	90	701
67	298	-19.667	-46.950	87.2	Araxa	Brazil	America South	90	201
68	496	51.517	12.200	89	Delitzsch	Germany	Europe	90	301
69	168	-18.150	26.867	89	Katete	Zimbabwe	Africa	90	701
70	3	-11.683	14.433	92	Catanda	Angola	Africa	90	701
71	262	48.433	-115.433	94	Rainy Creek	USA	America North	90	101
72	264	45.500	-113.333	95	Ravalli and Lemhi Counties	USA	America North	90	101
73	292	-17.500	-50.700	98	Santo Antonio Da Barra	Brazil	America South	100	201
74	311	-22.750	-56.250	98	Cerro Sarambi	Paraguay	America South	100	201
75	282	34.450	-92.867	99	Magnet Cove	USA	America North	100	101
76	304	-24.500	-49.200	103.1	Itapirapua	Brazil	America South	100	201
77	360	26.200	93.400	105	Samchampi	India	Asia	100	501
78	359	26.017	92.517	105.2	Jasra	India	Asia	110	501
79	159	-15.183	30.017	106.5	Kaluwe	Zambia	Africa	110	701

NN	ID Number	Lat (°)	Long (°)	Age (Ma)	Locality	Country	Continent	Reconstruction Age (Ma)	Plate ID
80	357	25.500	90.833	107	Swangkre	India	Asia	110	501
81	358	25.567	92.117	107	Sung Valley	India	Asia	110	501
82	329	34.750	117.200	110	Weishan	China	Asia	110	601
83	446	51.850	107.167	118	Khaluta	Russia	Asia	120	301
84	447	51.650	107.133	118	Arschan	Russia	Asia	120	301
85	448	51.917	107.483	118	Oshurkovo	Russia	Asia	120	301
86	6	-12.183	15.033	119	Monte Verde	Angola	Africa	120	701
87	230	45.500	-74.000	117	Oka	Canada	America North	120	101
88	445	51.933	107.067	122	Yuzhnoe	Russia	Asia	120	301
89	39	-15.117	34.917	123	Kangankunde	Malawi	Africa	120	701
90	308	-27.900	-49.150	132	Anitapolis*	Brazil	America South	130	201
91	78	-20.033	16.767	126.6	Okorusu	Namibia	Africa	130	701
92	328	36.500	117.833	127	Central Shandong Province	China	Asia	130	601
93	171	-19.750	32.300	127	Chishanya	Zimbabwe	Africa	130	701
94	310	-22.650	-55.950	128	Chiriguelo	Paraguay	America South	130	201
95	381	44.333	104.350	130.6	Bayan Khoshuu	Mongolia	Asia	130	410

NN	ID Number	Lat (°)	Long (°)	Age (Ma)	Locality	Country	Continent	Reconstruction Age (Ma)	Plate ID
96	300	-23.433	-47.600	127.7	Ipanema	Brazil	America South	130	201
97	47	-15.333	35.600	130.9	Chilwa Island	Malawi	Africa	130	701
98	303	-24.700	-48.133	131	Jacupiranga	Brazil	America South	130	201
99	26	22.050	33.617	131.6	Mansouri	Egypt	Africa	130	701
100	301	-24.183	-46.783	132.8	Itanhaem	Brazil	America South	130	201
101	11	-14.317	13.883	133	Tchivira-Bonga	Angola	Africa	130	701
102	48	-15.533	35.800	133	Tundulu	Malawi	Africa	130	701
103	84	-21.383	14.183	134	Messum	Namibia	Africa	130	701
104	452	58.400	119.067	134	Malomurunskii	Russia	Asia	130	301
105	324	38.333	110.833	134.8	Zijinshan	China	Asia	130	601
106	24	22.850	34.950	137.5	Nigrub el Fogani	Egypt	Africa	140	701
107	462	44.500	134.083	139	Koksharovskii	Russia	Asia	140	301
108	380	44.333	104.167	139.9	Mushgai Khudag	Mongolia	Asia	140	410
109	302	-24.383	-47.817	143	Juquia	Brazil	America South	140	201
110	25	22.700	34.467	146	El Naga	Egypt	Africa	150	701
111	255	62.667	-50.000	150	Frederikshabs Isblink	Greenland	America North	150	101

NN	ID Number	Lat (°)	Long (°)	Age (Ma)	Locality	Country	Continent	Reconstruction Age (Ma)	Plate ID
112	343	22.717	109.550	155	Mashan	China	Asia	150	601
113	256	61.900	-49.500	162	Ilulilarssuk	Greenland	America North	160	101
114	80	-20.800	16.117	163.2	Kalkfeld	Namibia	Africa	160	701
115	252	65.383	-51.700	172	Qaqarssuk	Greenland	America North	170	101
116	342	23.250	103.250	180.7	Jijie	China	Asia	180	601
117	330	34.667	110.167	181	Huayangchuan	China	Asia	180	601
118	228	45.467	-75.550	190	Francon Quarry - Orleans	Canada	America North	190	101
119	177	52.383	-118.883	202	Howard Creek	Canada	America North	200	101
120	331	34.333	110.000	206	Huanglongpu	China	Asia	210	601
121	170	-19.200	31.717	209	Shawa	Zimbabwe	Africa	210	701
122	385	21.950	59.650	220	Asseel	Oman	Arabia	220	503
123	425	70.000	102.117	220	Bor-Uryakh	Russia	Asia	220	401
124	384	42.983	105.533	222.2	Luugin gol	Mongolia	Asia	220	410
125	326	40.367	115.217	228	Fanshan	China	Asia	230	601
126	325	40.000	113.000	229	Datong	China	Asia	230	601
127	426	70.250	105.417	239	Magan	Russia	Asia	240	401

NN	ID Number	Lat (°)	Long (°)	Age (Ma)	Locality	Country	Continent	Reconstruction Age (Ma)	Plate ID
128	418	70.967	103.167	250	Odikhincha****	Russia	Asia	250	401
129	420	70.717	103.467	250	Kugda****	Russia	Asia	250	401
130	417	70.950	101.433	250	Guli**	Russia	Asia	250	401
131	53	20.500	0.000	262	Adrar Tadhak	Mali	Africa	260	701
132	337	32.500	109.833	264	Miaoya	China	Asia	260	601
133	338	31.833	110.333	265	Shaxiongdong	China	Asia	260	601
134	424	70.317	102.017	265	Dalbykha	Russia	Asia	260	401
135	457	59.933	136.883	310	Ozernyi	Russia	Asia	310	401
136	415	55.067	60.233	312	Ilmenogorskii	Russia	Asia	310	401
137	179	52.400	-119.150	325	Verity	Canada	America North	320	101
138	181	52.133	-119.183	328	Mud Lake	Canada	America North	330	101
139	449	54.117	112.450	329	Saizhenskii	Russia	Asia	330	401
140	318	39.500	79.000	332	Wajiltag	China	Asia	330	601
141	175	55.717	-124.417	340	Vergil	Canada	America North	340	101
142	173	56.450	-123.750	344	Aley	Canada	America North	340	101
143	178	52.400	-119.100	351	Paradise Lake	Canada	America North	350	101

NN	ID Number	Lat (°)	Long (°)	Age (Ma)	Locality	Country	Continent	Reconstruction Age (Ma)	Plate ID
144	185	51.500	-116.500	356.5	Ice River	Canada	America North	360	101
145	488	67.800	29.450	360	Sokli	Finland	Europe	360	301
146	400	67.417	32.800	364	Afrikanda	Russia	Asia	360	301
147	398	67.717	33.783	368	Khibiny	Russia	Asia	370	301
148	399	67.433	32.950	372	Ozernaya Varaka	Russia	Asia	370	301
149	406	66.583	34.450	373.1	Turiy Peninsula	Russia	Asia	370	301
150	393	68.717	32.133	385	Seblyavr	Russia	Asia	380	301
151	407	67.567	30.483	380	Kovdor***	Russia	Asia	380	301
152	409	66.800	30.117	391	Vuoriyarvi	Russia	Asia	390	301
153	519	57.967	-5.033	394	Borralan	United Kingdom	Europe	390	331
154	442	50.150	96.717	400	Chik	Russia	Asia	400	401
155	441	50.567	96.533	404	Kharly	Russia	Asia	400	401

The ages are corrected according with:
*Comin-Charmant and Gomes (2005).
**Kamo et al. (2003).
***Rukhlov and Bell (2010).
****Kogarko and Lebedev (in press).